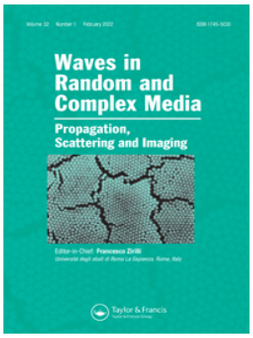

Waves in Random and Complex Media

ISSN: (Print) (Online) Journal homepage: https://www.tandfonline.com/loi/twrm20

Exact solutions for 2D boundary layer flow of two types of viscoelastic fluids and heat transfer on a permeable shrinking sheet with thermal radiation and variable surface temperature: existence of multiple solutions

Astick Banerjee, Krishnendu Bhattacharyya, Sanat Kumar Mahato, Ajeet Kumar Verma, Anil Kumar Gautam & Ali J. Chamkha

To cite this article: Astick Banerjee, Krishnendu Bhattacharyya, Sanat Kumar Mahato, Ajeet Kumar Verma, Anil Kumar Gautam & Ali J. Chamkha (2022): Exact solutions for 2D boundary layer flow of two types of viscoelastic fluids and heat transfer on a permeable shrinking sheet with thermal radiation and variable surface temperature: existence of multiple solutions, Waves in Random and Complex Media, DOI: 10.1080/17455030.2021.2023786

To link to this article: https://doi.org/10.1080/17455030.2021.2023786

Published online: 08 Feb 2022.

WAVES IN RANDOM AND COMPLEX MEDIA
https://doi.org/10.1080/17455030.2021.2023786

Taylor & Francis
Taylor & Francis Group

Exact solutions for 2D boundary layer flow of two types of viscoelastic fluids and heat transfer on a permeable shrinking sheet with thermal radiation and variable surface temperature: existence of multiple solutions

Astick Banerjee[a], Krishnendu Bhattacharyya [b], Sanat Kumar Mahato[a], Ajeet Kumar Verma[b], Anil Kumar Gautam[b] and Ali J. Chamkha[c]

[a]Department of Mathematics, Sidho-Kanho-Birsha University, Purulia, India; [b]Department of Mathematics, Institute of Science, Banaras Hindu University, Varanasi, India; [c]Faculty of Engineering, Kuwait College of Science and Technology, Doha District, Kuwait

ABSTRACT

A study with existence of multiple exact solutions has its own importance, and if the study is performed for a viscoelastic fluid, then the attraction becomes very high. So, here an attempt is performed, where the flow of two types of viscoelastic fluids and heat transfer due to shrinking of a permeable sheet is described. In the energy flow, the impacts of thermal radiation and variable temperature of the wall are simultaneously undertaken. By using similarity approach, in addition to single solution, the dual and triple closed-form solutions of the flow field and temperature are obtained in some specific flow situations of two fluids, namely, second-grade and Walters liquid B. Dual solutions for the flow of second-grade fluid are detected only for stronger mass suction with smaller viscoelastic parameter of second-grade fluid and for both weaker and stronger mass suctions (for two ranges) with larger viscoelastic parameter and unique solution in case of mass injection. However, for the flow of Walters liquid B, boundary layer solution is attained for mass suction only, and most importantly, triple solutions for some mass suction range are found. Now for heat flow, an exceptional result is witnessed: if the wall temperature distribution is assumed suitably, then the heat transfer rate is not dependent on the fluid rheology. Also, influences of involved physical parameters on velocity, temperature and other important quantities are described through some graphs.

ARTICLE HISTORY
Received 5 July 2021
Accepted 21 December 2021

KEYWORDS
Exact solutions; dual and triple solutions; viscoelastic fluids; permeable shrinking sheet; thermal radiation

1. Background

Viscoelastic fluid is a non-Newtonian fluid having the higher molecular weight, and for the elastic character with drag-reducing property, it has a tendency to flow in a laminar state. In addition, viscoelastic fluids have a certain microstructure, which makes those completely different from Newtonian fluids. Due to these, flows of viscoelastic fluid in boundary layer

CONTACT Krishnendu Bhattacharyya krish.math@yahoo.com

appear as an attractive topic of analysis for the researchers in theoretical, practical and application points of view. Besides flow nature, heat transfer in some viscoelastic fluids is much more interesting than that of in the Newtonian fluid, and the obvious reason behind it is the notable enhancement in heat transfer coefficient for those viscoelastic fluids.

Boundary layer structure of viscoelastic fluid flow has a unique standing due to its applications in numerous engineering and industrial problems because of lesser drag force. Some of those applications can be stated as drawing of plastic films, polymer extrusion, crystal growing, glass fiber production and so on. Our focus is concentrated on viscoelastic transport due to shrinking or expanding surfaces. The flow of viscoelastic fluid due to an expanding sheet was studied by Siddappa and Khapate [1] considering the Rivlin–Ericksen fluid model. While Walter's liquid B or second-order fluid flow (restriction on material modulus) caused by linearly stretching sheet was discussed by Rajagopal et al. [2] and Siddappa and Abel [3,4]. Later, the heat transfer analysis of the problem for Walter's liquid B was described by Dandapat and Gupta [5] for the steady case, and the unsteady case was illustrated by Ahmad et al. [6]. The effect of transverse magnetic field on the flow of Walter's liquid B was reported by Andersson [7]. Next, Cortell [8] obtained a similarity solution of heat transfer for CST and PST cases for the second-order fluid. Vajravelu and Roper [9] and Cortell [10] investigated the flow and heat transfer for viscoelastic fluid taking second-grade fluid model (no restriction on material modulus) over a stretching sheet. Later on, several important features of aforesaid flow of viscoelastic fluids were explored by Sarma and Rao [11], Ariel [12], Khan et al. [13], Hayat and Sajid [14], Cortell [15], Bataller [16], Abel et al. [17] and Chen [18] in their investigations. In a combined study, Cortell [19] presented the mass transfer phenomenon with chemical reaction in the flows of two viscoelastic fluids induced by a permeable stretching sheet. Magnetohydrodynamic (MHD) mixed convection in the viscoelastic fluid over an expanding sheet was conferred by Turkyilmazoglu [20] and Hayat et al. [21] explicated the effects of heterogeneous and homogeneous reactions on the viscoelastic fluid flow. Viscoelastic boundary layer flow due to shrinking sheet is much more interesting because here flow separation can be quite different from the Newtonian fluids, and it should be controlled somehow. Hayat et al. [22] obtained HAM (homotopy analysis method) solution for the MHD flow of second-grade fluid induced by a shrinking sheet. Later, Naganthran et al. [23] discussed the viscoelastic fluid flow near a stagnation point on a shrinking surface, and they described the stability of the obtained dual solutions. Along with these key investigations, there are important recent studies on the Newtonian fluid flow due to the shrinking sheet [24–31] exploring vital results, which are exclusively beneficial to engineering and industrial processes.

Exciting characters of the viscoelastic fluids and the flow due to shrinking sheet motivated us to explore some important results for the boundary layer viscoelastic fluid flow and heat transfer on a porous shrinking sheet with mass suction/injection. Here, two types of viscoelastic fluids are considered, and the flows are undertaken in the presence of thermal radiation and variable surface temperature. Unique, dual and triple exact solutions for velocity and temperature fields are found for certain conditions on the flow parameters and those are expressed in some figures and tables. This complete comparative study of solution existence for the aforesaid flow of two viscoelastic fluids (second-grade fluid and Walter's liquid B) with that of the Newtonian fluid is quite novel and yet to be reported. The existence of multiple solutions is confirmed using the Sturm functions analysis. Also, examination of the combined effects of thermal radiation and variable surface temperature

distribution on the heat transfer characteristics of the two viscoelastic flows explores new results. On the other hand, regarding applications, the study of viscoelastic flows is beneficial to many industries, like aerospace, automotive, rubber and oil industries [32] and viscoelastic jet flows also have applications to printing processes, scaffolds for tissue engineering and drug delivery systems for controlled drug release [33]. So, we feel that this investigation will contribute to the literature of viscoelastic flow in some aspects.

2. Flow formulation and solution

Let us consider the steady 2D laminar motion of incompressible viscoelastic fluids over a flat, horizontal porous shrinking sheet in the presence of wall mass transfer. The sheet coincides with the plane $y = 0$ and the flow region is the upper part of plane $y = 0$, i.e. the region $y > 0$. The fluid motion is caused due to the linear shrinking of the flat sheet with the application of two equal and reverse forces along the x-axis protecting the position of the origin. The steady two-dimensional boundary layer equations of motion of two viscoelastic fluids may be written, in usual notation, as follows [16,19]:

$$\frac{\partial u}{\partial x} + \frac{\partial u}{\partial y} = 0, \tag{1}$$

$$u\frac{\partial u}{\partial x} + v\frac{\partial u}{\partial y} = \upsilon\frac{\partial^2 u}{\partial y^2} \pm k_0\left[\frac{\partial u}{\partial x}\frac{\partial^2 u}{\partial y^2} + u\frac{\partial^3 u}{\partial x \partial y^2} - \frac{\partial u}{\partial y}\frac{\partial^2 u}{\partial x \partial y} + v\frac{\partial^3 u}{\partial y^3}\right], \tag{2}$$

where u and v are the components of velocity in x- and y-directions, respectively, υ is the kinematic viscosity and k_0 is the coefficient of viscoelasticity.

The positive sign in the right side of equation (2) corresponds to general second-grade fluid (Cortell [19]; $k_0 = \alpha_1/\rho; \alpha_1 \geq 0, \alpha_1$ being the material modulus), whereas the negative sign stands for Walter's liquid B or second-order fluid (Khan et al. [13]; $k_0 = -\alpha_1/\rho; \alpha_1 \leq 0$, α_1 being small). The boundary conditions are given by

$$u = -U_w(x) = -cx, \; v = -v_w \text{ at } y = 0, \tag{3}$$

$$u \to 0, \; \frac{\partial u}{\partial y} \to 0 \text{ as } y \to \infty, \tag{4}$$

where $U_w(= cx)$ is shrinking velocity with $c > 0$ being shrinking constant and v_w is the wall mass transfer velocity ($v_w > 0$ for mass suction and $v_w < 0$ for mass injection). The second condition in (4) is the augmented condition, since the flow is on the shrinking sheet, and it is a boundless domain, which had been already explained by Garg and Rajagopal [34].

Now, we introduce the similarity transformations:

$$\psi = \sqrt{\upsilon x U_w}\, f(\eta) \text{ and } \eta = y\sqrt{\frac{U_w}{x\upsilon}}, \tag{5}$$

where ψ is the stream function with $u = \frac{\partial \psi}{\partial y}$ & $v = -\frac{\partial \psi}{\partial x}$ and η is the similarity variable.

In view of relations in (5), we finally obtain following self-similar equations as follows:

$$f''' + ff'' - f'^2 - \alpha(f''^2 - 2f'f''' + ff'''') = 0, \tag{6}$$

where $\alpha = \pm ck_0/\upsilon$ is the viscoelastic parameter with $\alpha > 0$ corresponding to the second-grade fluid and $\alpha < 0$ for the Walter's liquid B (with $|\alpha| < 1$).

The boundary conditions reduce to the following forms:

$$f(0) = S, f'(0) = -1, f'(\infty) = 0, f''(\infty) = 0, \tag{7}$$

where $S = v_w/\sqrt{\upsilon c}$ is the wall mass transfer parameter. $S > 0$ ($v_w > 0$) corresponds mass suction and $S < 0$ ($v_w < 0$) corresponds mass injection.

The local skin-friction coefficient is given by $C_f = \frac{\tau_w}{\frac{1}{2}\rho U_w^2}$, where the wall shear stress τ_w on the surface is of the form [17]:

$$\tau_w = \rho\left[\upsilon\left(\frac{\partial u}{\partial y}\right) \pm k_0\left(2\frac{\partial u}{\partial x}\frac{\partial u}{\partial y} + u\frac{\partial^2 u}{\partial x \partial y}\right)\right]_{y=0}.$$

Thus, C_f is obtained as follows: $\frac{1}{2(1-3\alpha)}\sqrt{Re_x}C_f = f''(0)$, where $Re_x = U_w x/\upsilon$ is the local Reynolds number.

An exact closed-form solution of equation (6) with the transformed boundary conditions (7) can be obtained as follows:

$$f(\eta) = S - \frac{1}{\lambda} + \frac{1}{\lambda}e^{-\lambda\eta}, \tag{8}$$

where $\lambda(> 0)$ is a constant, which satisfies the following cubic equation:

$$\alpha S\lambda^3 + (1-\alpha)\lambda^2 - S\lambda + 1 = 0. \tag{9}$$

For $S = 0$, i.e. for nonporous shrinking sheet, equation (9) gives $\lambda = 1/\sqrt{\alpha - 1}$ (positive value only) and the solution for the corresponding flow becomes

$$f(\eta) = \sqrt{\alpha - 1}\left(e^{-\eta/\sqrt{\alpha-1}} - 1\right). \tag{10}$$

So, for nonporous shrinking sheet, the boundary layer self-similar solution exists only for the second-grade fluid with $\alpha > 1$ and no boundary layer similarity solution is possible for Walter's liquid B. Also, the solution for second-grade fluid is unique.

To obtain the roots of Equation (9), the aforementioned cubic equation in λ is converted into an incomplete cubic equation as follows:

$$t^3 + pt + q = 0, \tag{11}$$

where $\lambda = t - \frac{1-\alpha}{3\alpha S}$, $p = \frac{-3\alpha S^2 - (1-\alpha)^2}{3\alpha^2 S^2}$ and $q = \frac{2(1-\alpha)^3 + 9\alpha S^2(1-\alpha) + 27\alpha^2 S^2}{27\alpha^3 S^3}$.

The roots of incomplete cubic Equation (11) are expressed as follows:

$$t_1 = C + D,\ t_{2,3} = -\tfrac{1}{2}(C + D) \pm i\tfrac{\sqrt{3}}{2}(C - D),$$

where $C = \sqrt[3]{-\frac{q}{2} + \sqrt{E}}$, $D = \sqrt[3]{-\frac{q}{2} - \sqrt{E}}$, $i^2 = -1$, $E = (\frac{p}{3})^3 + (\frac{q}{2})^2$.

So, the expression of dimensionless velocity is $f'(\eta) = -e^{-\lambda\eta}$ and the local skin-friction coefficient $\frac{1}{2(1-3\alpha)}\sqrt{Re_x}C_f = f''(0) = \lambda$, where $\lambda(> 0)$ obeys the Equation (9).

The solution (8) of (6) and (7) is obtained taking the help of Equations (9) in λ and (11) in t for different values of α and S.

For $\alpha = 0$, i.e. for Newtonian fluid the Equation (9) becomes a quadratic equation of λ. It provides two/one positive values of λ when $S > 2/S = 2$ and correspondingly two/one solutions. Also, no solutions exist for $S < 2$. All these are exactly same as the analysis of Miklavčič and Wang [24].

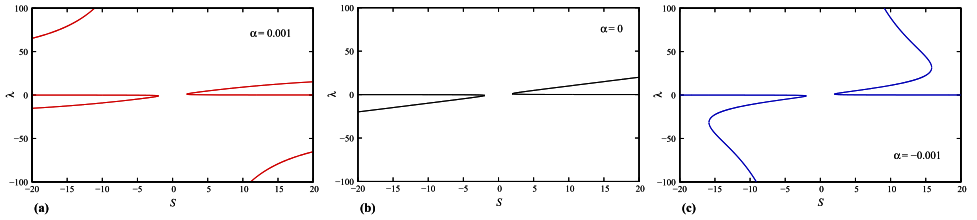

Figure 1. Comparison of values of λ vs. S for (a) second-grade fluid, (b) Newtonian fluid and (c) Walter's liquid B.

2.1. Comparison of solutions for three fluid models: second-grade fluid ($\alpha > 0$), Newtonian fluid ($\alpha = 0$) and Walter's liquid B ($\alpha < 0$)

The graphical comparison of the values of λ and the root of Equation (9) for three values of α is presented in Figure 1 for $-20 < S < 20$, where $\lambda > 0$ signifies the feasible solution. From the figures for three values of α for three types of fluids, namely, second-grade fluid ($\alpha = 0.001$), Newtonian fluid ($\alpha = 0$) and Walter's liquid B ($\alpha = -0.001$), a clear idea can be made on how the nature of solution changes for a slight change of values of α from the point $\alpha = 0$, i.e. in transition from Newtonian fluid to two types of non-Newtonian viscoelastic fluids. For Newtonian fluid ($\alpha = 0$), dual solutions are obtained in the presence of a certain amount of mass suction, and otherwise, no solution is observed. For the second-grade fluid ($\alpha = 0.001$), the existence of dual solution is exactly similar to that of a Newtonian fluid, but here a solo solution also exists for mass injection. On the other hand, for Walter's liquid B ($\alpha = -0.001$), triple solutions exist for a certain range of mass suction, and there is no solution for injection.

2.2. S-grade fluid ($\alpha > 0$)

The obtained roots of Equation (9), i.e. the values of λ are plotted in Figure 2 for various values of S and $\alpha(> 0)$ and the positive values of λ, i.e. the values of the skin-friction coefficient $\frac{1}{2(1-3\alpha)}\sqrt{Re_x}C_f = f''(0)$ are illustrated through Figure 3. Two types of nature for existence of solutions are obtained for different positive values of α in different ranges of S. In the first type, for small values of α (≤ 1), there exists dual solutions for S being equal or exceed some critical positive value, say, S_c, i.e. beyond a critical value of mass suction and as α increases up to 1 that critical value also increases. For any negative value of S, i.e. for mass injection, the solution is always unique. So, in $[0,S_c)$, no boundary layer solution for second-grade fluid with $\alpha \leq 1$ is found, and it confirms that for $S = 0$, the solutions exist only for $\alpha > 1$. In the next type, for values of $\alpha > 1$, two regions of S of dual solutions are obtained. One is similar to the first type, i.e. if S is greater than or equal to S_c and then two solutions are found and the other value of $S(> 0)$ must be less than or equal to some first critical positive value and let it be S_c^*, with $S_c^* < S_c$. It means that in $(0, S_c^*]$ solution is of dual nature for $\alpha > 1$ and similar to the first type for negative S, i.e. for mass injection, only one solution is observed. So, for this type, in (S_c^*, S_c), no similarity solution exists. The detail ranges of S, where single and dual solutions exist and where no solution is found, is presented in Table 1 for several values of α. The dimensionless velocity profiles are presented in Figures 4 and 5 for numerous values of α and S, and the nondimensional stream function for variations in α are demonstrated

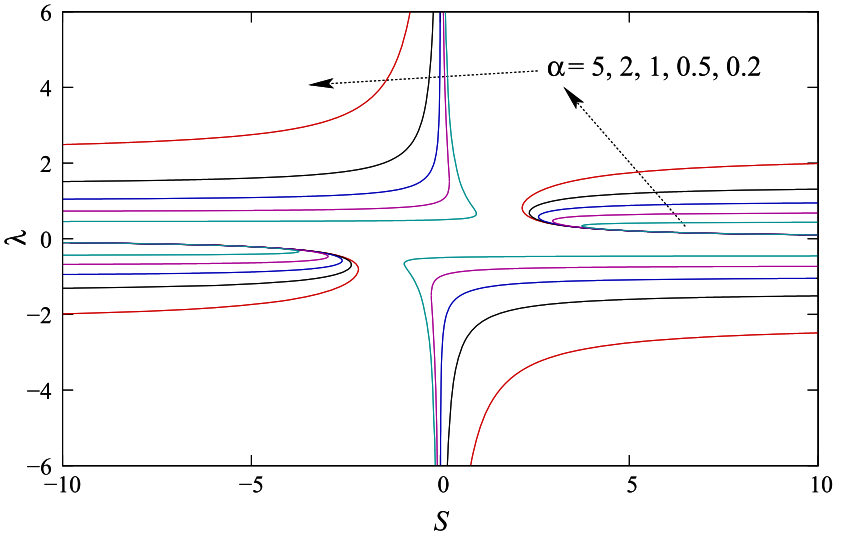

Figure 2. Solution domain of λ vs. S for various values of mass transfer parameter α (for second-grade fluid, $\alpha > 0$).

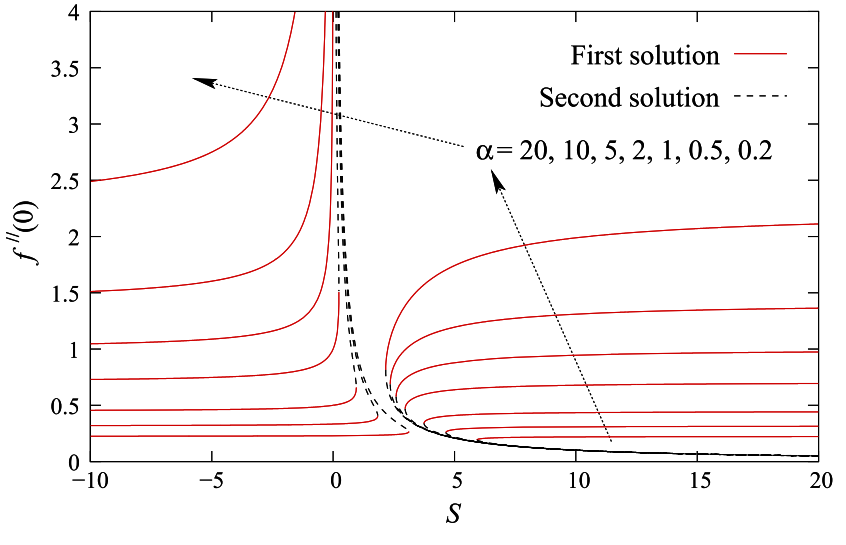

Figure 3. Skin-friction coefficient $\frac{1}{2(1-3\alpha)}\sqrt{Re_x}C_f = f''(0)$ vs. S for various values of mass transfer parameter α (for second-grade fluid, $\alpha > 0$).

in Figure 6. The boundary layer velocity shows the decreasing nature with α in two types of first solutions and single solution, which causes the increase in boundary layer thickness, and reverse results are found for second solutions. The stream function profiles also have similar variations like velocity due to change in α. However, with stronger mass suction, the velocity decreases for first solutions, and it reduces for second solutions. The unique velocity profiles exhibit the decreasing character for growing mass injection.

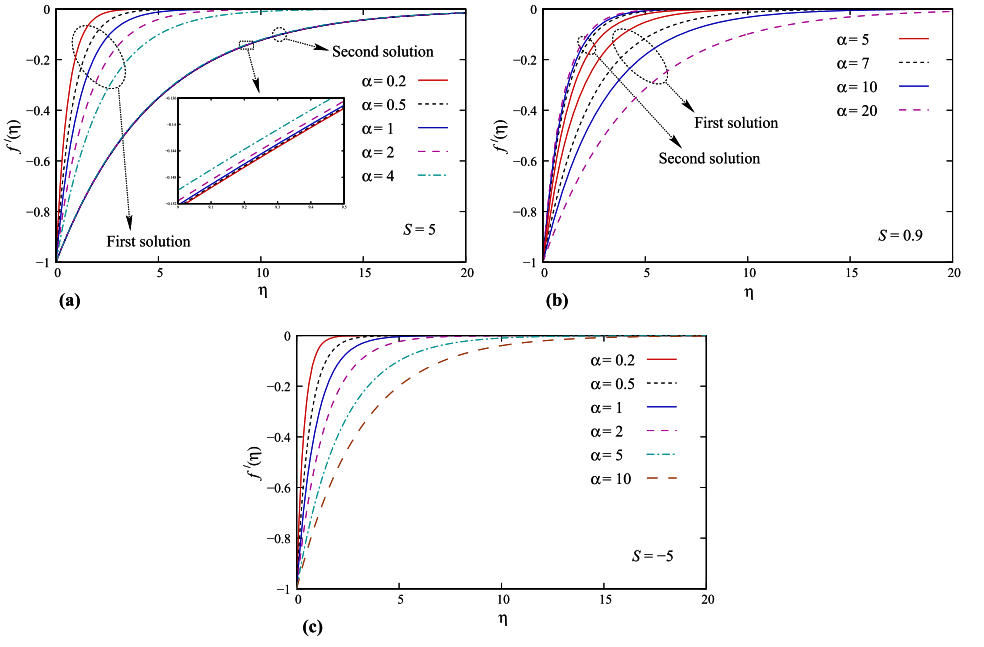

Figure 4. (a) Dual velocity profiles $f'(\eta)$ with $S = 5$, (b) dual velocity profiles $f'(\eta)$ with $S = 0.9$ and (c) single velocity profiles $f'(\eta)$ with $S = -5$ for various values of viscoelastic parameter α (for second-grade fluid case, $\alpha > 0$).

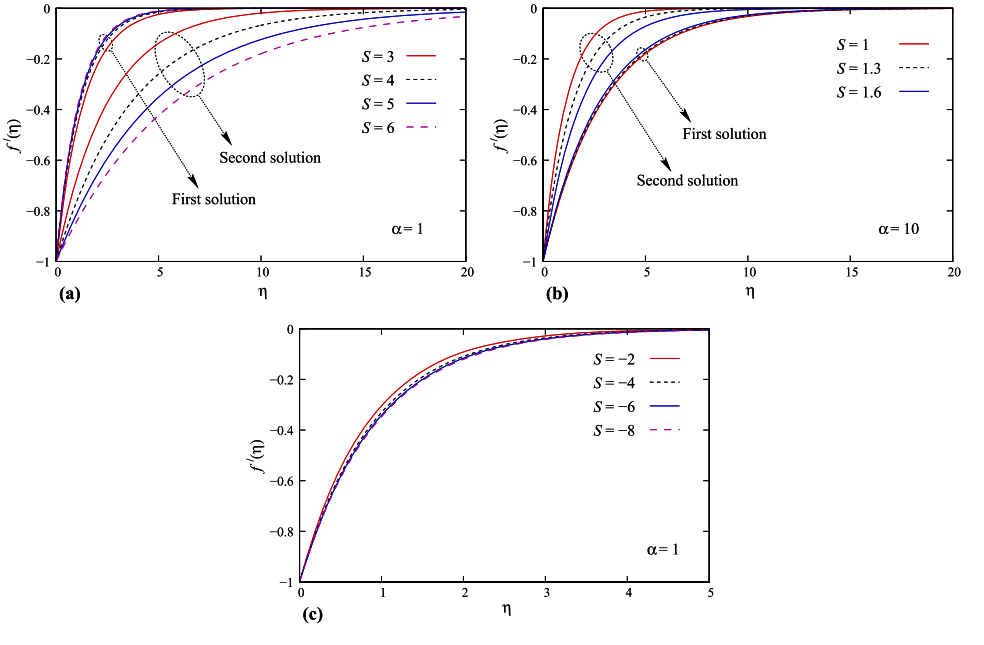

Figure 5. (a) Dual velocity profiles $f'(\eta)$ with $\alpha = 1$, (b) dual velocity profiles $f'(\eta)$ with $\alpha = 10$ and (c) single velocity profiles $f'(\eta)$ with $\alpha = 1$ for various values of mass transfer parameter S (for second-grade fluid, $\alpha > 0$).

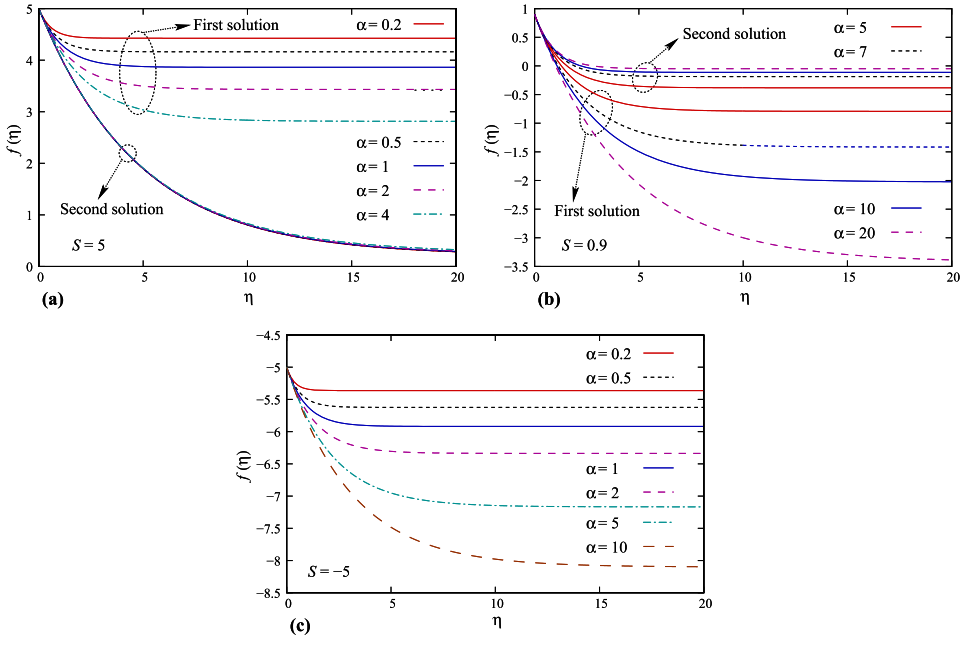

Figure 6. (a) Dual dimensionless stream function profiles $f(\eta)$ with $S = 5$, (b) dual dimensionless stream function profiles $f(\eta)$ with $S = 0.9$ and (c) single-dimensionless stream function profiles $f(\eta)$ with $S = -5$ for various values of viscoelastic parameter α (for second-grade fluid, $\alpha > 0$).

Table 1. The critical values and ranges of S for which dual, single and no solutions exist for second-grade fluid.

	Critical values of S		Ranges of S with		
α	S_c	S_c^*	Single solution	Dual solutions	No solution
0.2	2.16685	–	(−∞,0)	[2.16685,∞)	[0,2.16685)
0.5	2.35481	–	(−∞,0)	[2.35481,∞)	[0,2.35481)
1	2.59808	–	(−∞,0)	[2.59808,∞)	[0,2.59808)
1.001	2.59851	0.00001	(−∞,0]	[2.59851,∞) & (0,0.00001]	(0.00001,2.59851)
1.01	2.60241	0.00038	(−∞,0]	[2.60241,∞) & (0,0.00038]	(0.00038,2.60241)
1.05	2.61953	0.00416	(−∞,0]	[2.61953,∞) & (0,0.00416]	(0.00416,2.61953)
1.1	2.64057	0.01141	(−∞,0]	[2.64057,∞) & (0,0.01141]	(0.01141,2.64057)
1.2	2.68156	0.03044	(−∞,0]	[2.68156,∞) & (0,0.03044]	(0.03044,2.68156)
1.5	2.79691	0.10320	(−∞,0]	[2.79691,∞) & (0,0.10320]	(0.10320,2.79691)
2	2.96957	0.23811	(−∞,0]	[2.96957,∞) & (0,0.23811]	(0.23811,2.96957)
3	3.26599	0.50000	(−∞,0]	[3.26599,∞) & (0,0.50000]	(0.49999,3.26599)
4	3.52035	0.73801	(−∞,0]	[3.52035,∞) & (0,0.73801]	(0.73801,3.52035)
5	3.74676	0.95488	(−∞,0]	[3.74676,∞) & (0,0.95488]	(0.95488,3.74676)
10	4.64758	1.83711	(−∞,0]	[4.64758,∞) & (0,1.83711]	(1.83711,4.64758)
20	5.93816	3.11863	(−∞,0]	[5.93816,∞) & (0,3.11863]	(3.11863,5.93816)

2.3. Walter's liquid B ($\alpha < 0$)

The values of λ and the skin-friction coefficient are depicted in Figures 7 and 8, respectively, for different values of α (< 0 with $|\alpha| < 1$) and S. For Walter's liquid B, the solution is only obtained for mass suction, and there is no solution for mass injection. Interestingly, here some smaller negative values of α triple solutions exist in a certain range of S, say (S_w^*, S_w).

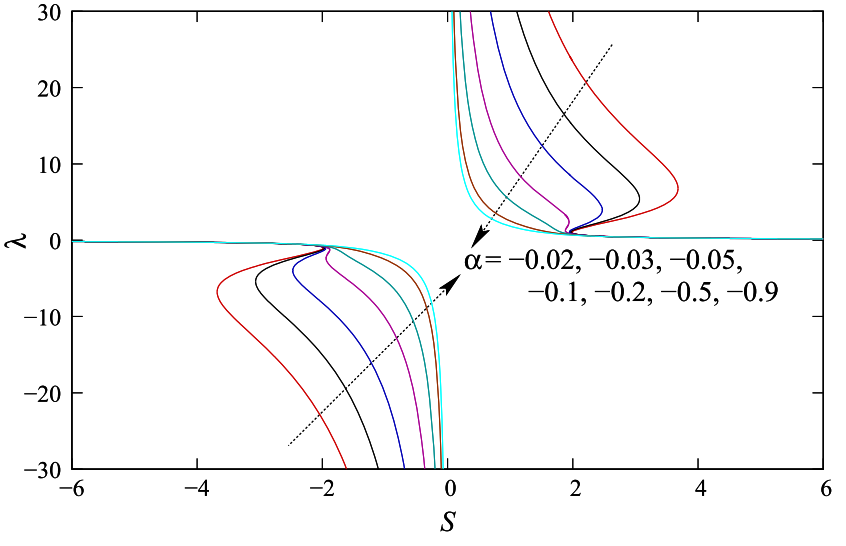

Figure 7. Solution domain of λ vs. S for various values of viscoelastic parameter α (for Walter's liquid B, $\alpha < 0$).

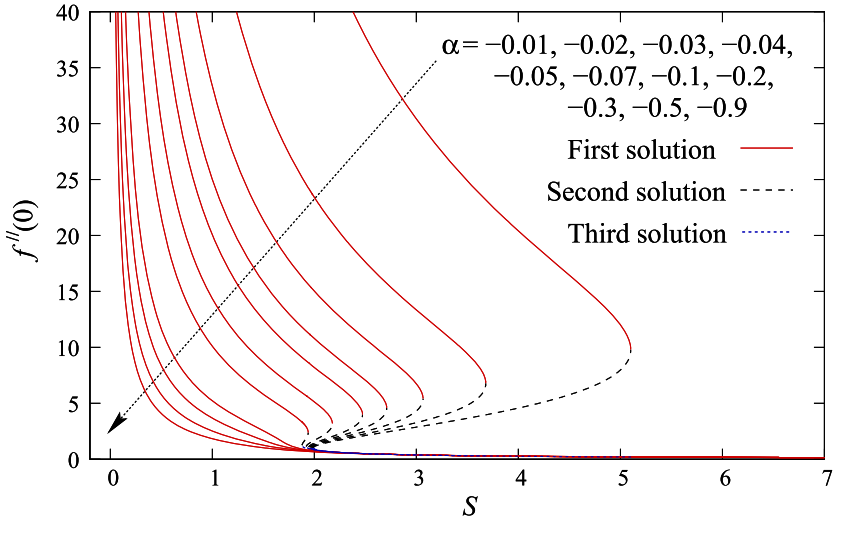

Figure 8. Skin-friction coefficient $\frac{1}{2(1-3\alpha)}\sqrt{Re_x}C_f = f''(0)$ vs. S for various values of viscoelastic parameter α (for Walter's liquid B, $\alpha < 0$).

So, there exist two critical values S_w^* and S_w, and if the amount of mass suction is considered in between those, then triple solutions are found, otherwise the solution is unique. It is worthwhile to note that when the negative value of α becomes slightly higher in magnitude ($\alpha \leq -0.13$), then the solution also turns out to be unique in nature for all values of suction. The existence and uniqueness of solutions in various ranges of S are presented in Table 2 for several values of α. The triple and single velocity profiles are demonstrated in Figures

Table 2. The critical values and ranges of S for which triple, single and no solutions exist for Walter's liquid B.

	Critical values of S		Ranges of S with		
α	S_w^*	S_w	Single solution	Triple solutions	No solution
−0.01	1.98986	5.10101	(0,1.98986) & (5.10101,∞)	[1.98986,5.10101]	(−∞,0]
−0.015	1.98470	4.20685	(0,1.98470) & (4.20685,∞)	[1.98470,4.20685]	(−∞,0]
−0.02	1.97947	3.67990	(0,1.97947) & (3.67990,∞)	[1.97947,3.67990]	(−∞,0]
−0.03	1.96877	3.06550	(0,1.96877) & (3.06550,∞)	[1.96877,3.06550]	(−∞,0]
−0.04	1.95773	2.70875	(0,1.95773) & (2.70875,∞)	[1.95773,2.70875]	(−∞,0]
−0.05	1.94631	2.47222	(0,1.94631) & (2.47222,∞)	[1.94631,2.47222]	(−∞,0]
−0.07	1.92212	2.17643	(0,1.92212) & (2.17643,∞)	[1.92212,2.17643]	(−∞,0]
−0.1	1.88101	1.93953	(0,1.88101) & (1.93953,∞)	[1.88101,1.93953]	(−∞,0]
−0.11	1.86525	1.89039	(0,1.86525) & (1.89039,∞)	[1.86525,1.89039]	(−∞,0]
−0.12	1.84752	1.85202	(0,1.84752) & (1.85202,∞)	[1.84752,1.85202]	(−∞,0]
−0.124	1.83939	1.83977	(0,1.83939) & (1.83977,∞)	[1. 83939,1.83977]	(−∞,0]
−0.1249	1.837357	1.837368	(0,1.837357) & (1.837368,∞)	[1.837357,1.837368]	(−∞,0]
−0.12499	1.8371416	1.8371420	(0,1.83714161) & (1.83714199,∞)	[1.83714161,1.83714199]	(−∞,0]
−0.125	–	–	(0,∞)	–	(−∞,0]
−0.13	–	–	(0,∞)	–	(−∞,0]
−0.15	–	–	(0,∞)	–	(−∞,0]
−0.2	–	–	(0,∞)	–	(−∞,0]
−0.5	–	–	(0,∞)	–	(−∞,0]
−0.9	–	–	(0,∞)	–	(−∞,0]

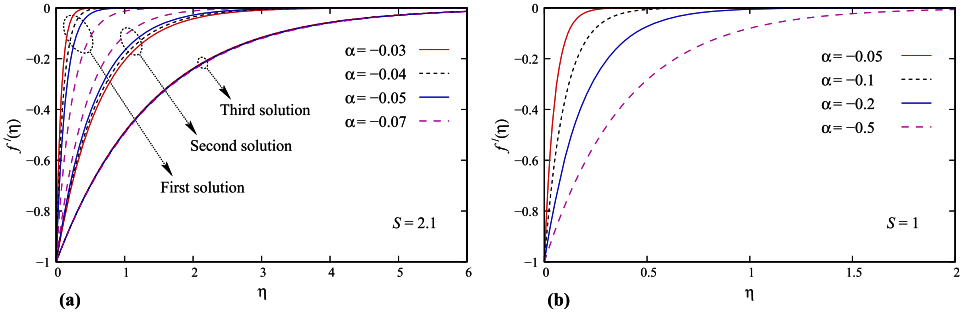

Figure 9. (a) Triple velocity profiles $f'(\eta)$ with $S = 2.1$ and (b) single velocity profiles $f'(\eta)$ with $S = 1$ for various values of viscoelastic parameter α (for Walter's liquid B case, $\alpha < 0$).

9 and 10, respectively, for different α and S, and dimensionless stream functions are plotted in Figure 11 for some values of α. The first solution and third solution show the similar behavior, and in the second, the effects are just opposite. Due to the increase in magnitude of α and S, the velocity inside the boundary layer reduces for both first and third solutions, and it enhances for second solution. Also, a reduction in stream function profiles (Figure 11) is found in first and third solutions with the increasing magnitude of α.

2.4. Confirmation of existence of positive root (λ) using Sturm functions

Equation (9) of λ is a polynomial equation with real coefficient. So, it is quite convenient and easy way to confirm the exact number of real roots (positive and negative) without multiplicity by the method of Sturm functions. Let $h(\lambda) = \alpha S\lambda^3 + (1-\alpha)\lambda^2 - S\lambda + 1$, where α and S are known. Then, $h(\lambda) = 0$ becomes Equation (9), and the corresponding strum

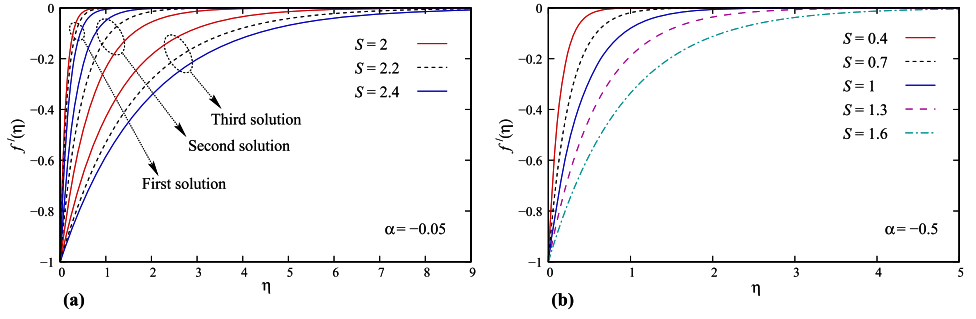

Figure 10. (a) Triple velocity profiles $f'(\eta)$ with $\alpha = -0.05$ and (b) single velocity profiles $f'(\eta)$ with $\alpha = -0.5$ for various values of mass transfer parameter S (for Walter's liquid B, $\alpha < 0$).

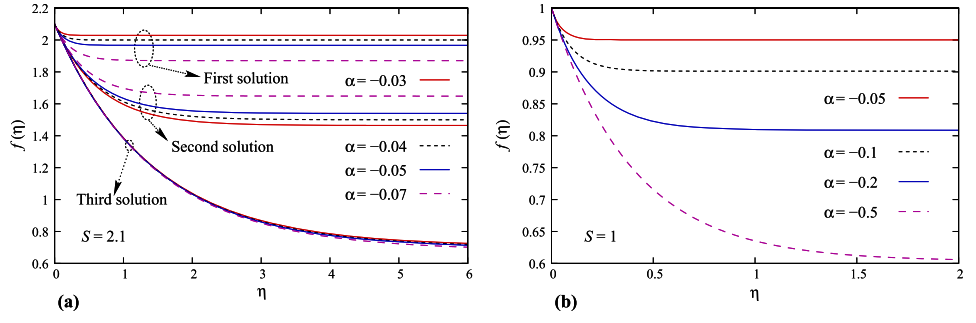

Figure 11. (a) Triple dimensionless stream function profiles $f(\eta)$ with $S = 2.1$ and (b) single-dimensionless stream function profiles $f(\eta)$ with $S = 1$ for various values of viscoelastic parameter α (for Walter's liquid B, $\alpha < 0$).

functions are as follows:

$$h(\lambda) = \alpha S\lambda^3 + (1-\alpha)\lambda^2 - S\lambda + 1,$$

$$h_1(\lambda) = 3\alpha S\lambda^2 + 2(1-\alpha)\lambda - S,$$

$$h_2(\lambda) = \left(\frac{2S}{3} + \frac{2}{9\alpha S} + \frac{2\alpha}{9S} - \frac{4}{9S}\right)\lambda - \left(\frac{8}{9} + \frac{1}{9\alpha}\right),$$

$$h_3(\lambda) = S + \frac{8\alpha - 7 - 1/\alpha}{\left(3S + \frac{1}{\alpha S} + \frac{\alpha}{S} - \frac{2}{S}\right)} - \frac{16\alpha S + 4S + S/4\alpha}{\frac{1}{3}\left(3S + \frac{1}{\alpha S} + \frac{\alpha}{S} - \frac{2}{S}\right)^2}.$$

Sequences of signs of strum functions for $\lambda = -\infty, 0, \infty$ are presented in Table 3 for some values of α and S and obvious conclusions on the existence of positive and negative roots are made. Those obtained ranges and critical values of S for different α (for both second-grade fluid and Walter's liquid B) are identically same as found in calculating the roots of Equation (9).

Table 3. Signs of strum functions of equation (9) for several values of α and S to confirm real roots.

			Signs of strum functions					
α	S	λ	$h(\lambda)$	$h_1(\lambda)$	$h_2(\lambda)$	$h_3(\lambda)$	Total number of changes in sign	Exact number of real root(s)
1	> 0	$-\infty$	$-$	$+$	$-$	$+/-$ [($S \geq 2.59808$)/ otherwise]	3/2	1 negative root and 2/0 positive root(s) as $S \geq$ / < 2.59808
		0	$+$	$-$	$-$	$+/-$ [($S \geq 2.59808$)/ otherwise]	2/1	
		∞	$+$	$+$	$+$	$+/-$ [($S \geq 2.59808$)/ otherwise]	0/1	
	< 0	$-\infty$	$+$	$-$	$+$	$-/+$ [($S \leq -2.59808$)/ otherwise]	3/2	2/0 negative root(s) as $S \leq$ / > 2.59808 and 1 positive root
		0	$+$	$+$	$-$	$-/+$ [($S \leq -2.59808$)/ otherwise]	1/2	
		∞	$-$	$-$	$-$	$-/+$ [($S \leq -2.59808$)/ otherwise]	0/1	
1.001	> 0	$-\infty$	$-$	$+$	$-$	$+/-$ [($0 < S \leq 0.00001$ and $S \geq 2.59851$)/ otherwise]	3/2	1 negative root and 2/0 positive root(s) as ($0 < S \leq 0.00001$ and $S \geq 2.59851$)/ otherwise
		0	$+$	$-$	$-$	$+/-$ [($0 < S \leq 0.00001$ and $S \geq 2.59851$)/ otherwise]	2/1	
		∞	$+$	$+$	$+$	$+/-$ [($0 < S \leq 0.00001$ and $S \geq 2.59851$)/ otherwise]	0/1	
	< 0	$-\infty$	$+$	$-$	$+$	$-/+$ [($0 > S \geq -0.00001$ and $S \leq -2.59851$)/ otherwise]	3/2	2/0 negative root(s) as ($0 > S \geq -0.00001$ and $S \leq -2.59851$)/ otherwise and 1 positive root
		0	$+$	$+$	$-$	$-/+$ [($0 > S \geq -0.00001$ and $S \leq -2.59851$)/ otherwise]	1/2	
		∞	$-$	$-$	$-$	$-/+$ [($0 > S \geq -0.00001$ and $S \leq -2.59851$)/ otherwise]	0/1	

(*continued*).

Table 3. Continued.

			Signs of strum functions					
α	S	λ	$h(\lambda)$	$h_1(\lambda)$	$h_2(\lambda)$	$h_3(\lambda)$	Total number of changes in sign	Exact number of real root(s)
1.2	> 0	$-\infty$	$-$	$+$	$-$	$+/-$ [(0 $<$ $S \leq$ 0.03044 and $S \geq$ 2.68156)/ otherwise]	3/2	1 negative root and 2/0 positive root(s) as (0 $<$ $S \leq$ 0.03044 and $S \geq$ 2.68156)/ otherwise
		0	$+$	$-$	$-$	$+/-$ [(0 $<$ $S \leq$ 0.03044 and $S \geq$ 2.68156)/ otherwise]	2/1	
		∞	$+$	$+$	$+$	$+/-$ [(0 $<$ $S \leq$ 0.03044 and $S \geq$ 2.68156)/ otherwise]	0/1	
	< 0	$-\infty$	$+$	$-$	$+$	$-/+$ [(0 $>$ $S \geq -$0.03044 and $S \leq -$2.68156)/ otherwise]	3/2	2/0 negative root(s) as (0 $>$ $S \geq -$0.03044 and $S \leq -$2.68156)/ otherwise and 1 positive root
		0	$+$	$+$	$-$	$-/+$ [(0 $>$ $S \geq -$0.03044 and $S \leq -$2.68156)/ otherwise]	1/2	
		∞	$-$	$-$	$-$	$-/+$ [(0 $>$ $S \geq -$0.03044 and $S \leq -$2.68156)/ otherwise]	0/1	
$-$0.02	> 0	$-\infty$	$+$	$-$	$+$	$-/+$ [(1.97947 $\leq$ $S \leq$ 3.67990)/ otherwise]	3/2	No negative root and 3/1 positive root(s) as (1.97947 $\leq$ $S \leq$ 3.67990)/ otherwise
		0	$+$	$-$	$+$	$-/+$ [(1.97947 $\leq$ $S \leq$ 3.67990)/ otherwise]	3/2	
		∞	$-$	$-$	$-$	$-/+$ (1.97947 $\leq$ $S \leq$ 3.67990)/ otherwise	0/1	
	< 0	$-\infty$	$-$	$+$	$-$	$+/-$ [($-$1.97947 $\geq$ $S \geq$ $-$3.67990)/otherwise]	3/2	3/1 negative root(s) as ($-$1.97947 $\geq$ $S \geq$ $-$3.67990)/otherwise and no positive root
		0	$+$	$+$	$+$	$+/-$ [($-$1.97947 $\geq$ $S \geq$ $-$3.67990)/ otherwise]	0/1	
		∞	$+$	$+$	$+$	$+/-$ [($-$1.97947 $\geq$ $S \geq$ $-$3.67990)/ otherwise]	0/1	

(*continued*).

Table 3. Continued.

			Signs of strum functions					
α	S	λ	$h(\lambda)$	$h_1(\lambda)$	$h_2(\lambda)$	$h_3(\lambda)$	Total number of changes in sign	Exact number of real root(s)
-0.1	>0	$-\infty$	$+$	$-$	$+$	$-/+$ [$(1.88101 \leq S \leq 1.93953)$/ otherwise]	3/2	No negative root and 3/1 positive root(s) as $(1.88101 \leq S \leq 1.93953)$/ otherwise
		0	$+$	$-$	$+$	$-/+$ [$(1.88101 \leq S \leq 1.93953)$/ otherwise]	3/2	
		∞	$-$	$-$	$-$	$-/+$ [$(1.88101 \leq S \leq 1.93953)$/ otherwise]	0/1	
	<0	$-\infty$	$-$	$+$	$-$	$+/-$ [$(-1.88101 \geq S \geq -1.93953)$/ otherwise]	3/2	3/1 negative root(s) as $(-1.88101 \geq S \geq -1.93953)$/otherwise and no positive root
		0	$+$	$+$	$+$	$+/-$ [$(-1.88101 \geq S \geq -1.93953)$/ otherwise]	0/1	
		∞	$+$	$+$	$+$	$+/-$ [$(-1.88101 \geq S \geq -1.93953)$/ otherwise]	0/1	
$-0.124\,99$	>0	$-\infty$	$+$	$-$	$+$	$-/+$ [$(1.83714161 \leq S \leq 1.83714199)$/ otherwise]	3/2	No negative root and 3/1 positive root(s) as $(1.83714161 \leq S \leq 1.83714199)$/otherwise
		0	$+$	$-$	$+$	$-/+$ [$(1.83714161 \leq S \leq 1.83714199)$/otherwise]	3/2	
		∞	$-$	$-$	$-$	$-/+$ [$(1.83714161 \leq S \leq 1.83714199)$/otherwise]	0/1	

(*continued*).

Table 3. Continued.

			Signs of strum functions					
α	S	λ	$h(\lambda)$	$h_1(\lambda)$	$h_2(\lambda)$	$h_3(\lambda)$	Total number of changes in sign	Exact number of real root(s)
	< 0	$-\infty$	$-$	$+$	$-$	$+/-$ $(-1.83714161 \geq S \geq -1.83714199)$/otherwise	3/2	3/1 negative root(s) as $(-1.83714161 \geq S \geq -1.83714199)$/otherwise and no positive root
		0	$+$	$+$	$+$	$+/-$ $[(-1.83714161 \geq S \geq -1.83714199)$/otherwise]	0/1	
		∞	$+$	$+$	$+$	$+/-$ $[(-1.83714161 \geq S \geq -1.83714199)$/otherwise]	0/1	
-0.125	> 0	$-\infty$	$+$	$-$	$+/-$ $[(S \leq 1.837117307)/(S \geq 1.837117308)]$	$+$	2/2	No negative root and 1 positive root
		0	$+$	$-$	0	$+$	2	
		∞	$-$	$-$	$+/-$ $[(S \leq 1.837117307)/(S \geq 1.837117308)]$	$+$	1/1	
	< 0	$-\infty$	$-$	$+$	$-/+$ $[(S \geq -1.837117307)/(S \leq -1.837117308)]$	$-$	2/2	1 negative root and no positive root
		0	$+$	$+$	0	$-$	1	
		∞	$+$	$+$	$-/+$ $[(S \geq -1.837117307)/(S \leq -1.837117308)]$	$-$	1/1	

3. Heat transfer analysis

To be acquainted with the heat transfer characteristics with thermal radiation effect and variable surface temperature for the above flow of two types of viscoelastic fluids, the following boundary layer equation of energy (without viscous dissipation) needs to be solved:

$$u\frac{\partial T}{\partial x}+v\frac{\partial T}{\partial y}=\frac{\kappa}{\rho c_p}\frac{\partial^2 T}{\partial y^2}-\frac{1}{\rho c_p}\frac{\partial q_r}{\partial y}, \tag{12}$$

where T is the temperature, κ is the thermal conductivity, c_p is the specific heat and q_r is the radiative heat flux.

The appropriate boundary conditions are as follows:

$$T=T_w=T_\infty+T_0x^m \text{ at } y=0;\ T\to T_\infty \text{ as } y\to\infty, \tag{13}$$

where T_w is the variable temperature along the sheet, T_0 is a constant depending on the thermal properties of the fluid, T_∞ is the static temperature of free stream flow and m is a power-law exponent.

By using Rosseland's approximation for radiation [35], $q_r=-\frac{4\sigma}{3k_1}\frac{\partial T^4}{\partial y}$ is obtained, where σ is the Stefan-Boltzman constant and k_1 is the absorption coefficient. It is presumed that the variation in temperature within the flow field is such that T^4 may be expanded in Taylor's series. Expanding T^4 about T_∞ and neglecting higher-order terms, we get $T^4\approx 4T_\infty^3T-3T_\infty^4$.

Hence, the radiative heat flux may be rewritten as follows [35,36]:

$$q_r=-\frac{4\sigma}{3k_1}\frac{\partial T^4}{\partial y}=-\frac{16\sigma T_\infty^3}{3k_1\rho c_p}\frac{\partial^2 T}{\partial y^2}$$

and consequently, Equation (12) reduces to

$$u\frac{\partial T}{\partial x}+v\frac{\partial T}{\partial y}=\frac{\kappa}{\rho c_p}\frac{\partial^2 T}{\partial y^2}+\frac{16\sigma T_\infty^3}{3k_1\rho c_p}\frac{\partial^2 T}{\partial y^2}. \tag{14}$$

Next, the dimensionless temperature θ is introduced as follows:

$$\theta(\eta)=\frac{T-T_\infty}{T_w-T_\infty}. \tag{15}$$

By using the relations in (5) and (15), Equation (12) reduces to

$$(1+\tfrac{4}{3}Nr)\theta''+\Pr(f\theta'-mf'\theta)=0, \tag{16}$$

where $\Pr=\frac{\upsilon\rho c_p}{\kappa}$ is the well-known Prandtl number and $Nr=\frac{4\sigma T_\infty^3}{\kappa k_1}$ is the thermal radiation parameter.

The boundary conditions (13) become

$$\theta(\eta)=1 \text{ at } \eta=0;\ \theta(\eta)\to 0 \text{ as } \eta\to\infty \tag{17}$$

The local Nusselt number is defined as follows [18]:

$Nu_x=\frac{xq_w}{\kappa(T_w-T_\infty)}$, where q_w is the surface heat flux and $q_w=-\kappa\left(\frac{\partial T}{\partial y}\right)_{y=0}$.

Thus, the local Nusselt number Nu_x is given by $Nu_x Re_x^{-1/2} = -\theta'(0)$.

Using the solution (8) of (6) and (7), Equation (16) becomes

$$\theta'' + \frac{\mathrm{Pr}}{(1+\frac{4}{3}Nr)}\left(S - \frac{1}{\lambda} + \frac{1}{\lambda}e^{-\lambda\eta}\right)\theta' + \frac{m\,\mathrm{Pr}}{(1+\frac{4}{3}Nr)}e^{-\lambda\eta}\theta = 0. \tag{18}$$

Now, a new variable $\xi = \frac{\mathrm{Pr}}{(1+\frac{4}{3}Nr)\lambda^2}e^{-\lambda\eta}$ is introduced, and so Equation (18) reduces to

$$\xi\frac{d^2\theta}{d\xi^2} + (h-\xi)\frac{d\theta}{d\xi} - g\theta = 0, \tag{19}$$

where $h = 1 - \frac{\mathrm{Pr}}{(1+\frac{4}{3}Nr)\lambda}\left(S - \frac{1}{\lambda}\right)$ and $g = -m$.

The boundary conditions are as follows:

$$\theta\left(\frac{\mathrm{Pr}}{(1+\frac{4}{3}Nr)\lambda^2}\right) = 1 \text{ and } \theta(0) = 0. \tag{20}$$

The solution of the confluent hypergeometric Equation (19) with boundary conditions (20) is given by [37]:

$$\theta(\xi) = \frac{\left(\frac{(1+\frac{4}{3}Nr)\lambda^2}{\mathrm{Pr}}\xi\right)^{\frac{\mathrm{Pr}}{(1+\frac{4}{3}Nr)\lambda}\left(S-\frac{1}{\lambda}\right)} M\left(\frac{\mathrm{Pr}}{(1+\frac{4}{3}Nr)\lambda}\left(S-\frac{1}{\lambda}\right) - m, 1 + \frac{\mathrm{Pr}}{(1+\frac{4}{3}Nr)\lambda}\left(S-\frac{1}{\lambda}\right), \xi\right)}{M\left(\frac{\mathrm{Pr}}{(1+\frac{4}{3}Nr)\lambda}\left(S-\frac{1}{\lambda}\right) - m, 1 + \frac{\mathrm{Pr}}{(1+\frac{4}{3}Nr)\lambda}\left(S-\frac{1}{\lambda}\right), \frac{\mathrm{Pr}}{(1+\frac{4}{3}Nr)\lambda^2}\right)}, \tag{21}$$

where M is the confluent hypergeometric function of the first kind or Kummer function.

Thus, the dimensionless temperature, i.e. the solution of Equation (16) becomes

$$\theta(\eta) = \frac{e^{-\frac{\mathrm{Pr}}{(1+\frac{4}{3}Nr)}\left(S-\frac{1}{\lambda}\right)\eta} M\left(\frac{\mathrm{Pr}}{(1+\frac{4}{3}Nr)\lambda}\left(S-\frac{1}{\lambda}\right) - m, 1 + \frac{\mathrm{Pr}}{(1+\frac{4}{3}Nr)\lambda}\left(S-\frac{1}{\lambda}\right), \frac{\mathrm{Pr}}{(1+\frac{4}{3}Nr)\lambda^2}e^{-\lambda\eta}\right)}{M\left(\frac{\mathrm{Pr}}{(1+\frac{4}{3}Nr)\lambda}\left(S-\frac{1}{\lambda}\right) - m, 1 + \frac{\mathrm{Pr}}{(1+\frac{4}{3}Nr)\lambda}\left(S-\frac{1}{\lambda}\right), \frac{\mathrm{Pr}}{(1+\frac{4}{3}Nr)\lambda^2}\right)}, \tag{22}$$

where λ satisfies the cubic Equation (9).

So, the local Nusselt number is given as follows

$$Nu_x \mathrm{Re}_x^{-1/2} = -\theta'(0) = \frac{\mathrm{Pr}}{(1+\frac{4}{3}Nr)}\left(S - \frac{1}{\lambda}\right) + \frac{\mathrm{Pr}}{(1+\frac{4}{3}Nr)\lambda}\left(\frac{\frac{\mathrm{Pr}}{(1+\frac{4}{3}Nr)\lambda}\left(S-\frac{1}{\lambda}\right) - m}{1 + \frac{\mathrm{Pr}}{(1+\frac{4}{3}Nr)\lambda}\left(S-\frac{1}{\lambda}\right)}\right)$$
$$\times \frac{M\left(1 + \frac{\mathrm{Pr}}{(1+\frac{4}{3}Nr)\lambda}\left(S-\frac{1}{\lambda}\right) - m, 2 + \frac{\mathrm{Pr}}{(1+\frac{4}{3}Nr)\lambda}\left(S-\frac{1}{\lambda}\right), \frac{\mathrm{Pr}}{(1+\frac{4}{3}Nr)\lambda^2}\right)}{M\left(\frac{\mathrm{Pr}}{(1+\frac{4}{3}Nr)\lambda}\left(S-\frac{1}{\lambda}\right) - m, 1 + \frac{\mathrm{Pr}}{(1+\frac{4}{3}Nr)\lambda}\left(S-\frac{1}{\lambda}\right), \frac{\mathrm{Pr}}{(1+\frac{4}{3}Nr)\lambda^2}\right)}.$$

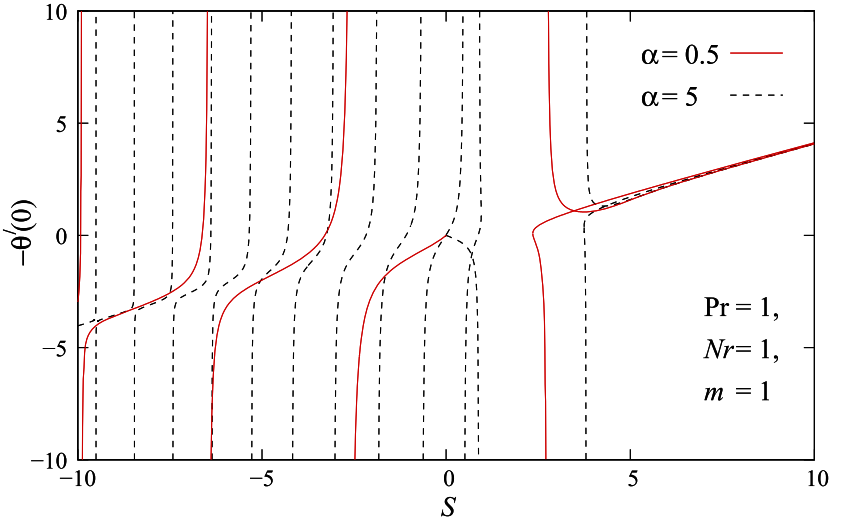

Figure 12. Nusselt number $Nu_x Re_x^{-1/2} = -\theta'(0)$ vs. S for various values of viscoelastic parameter α (for the second-grade fluid, $\alpha > 0$).

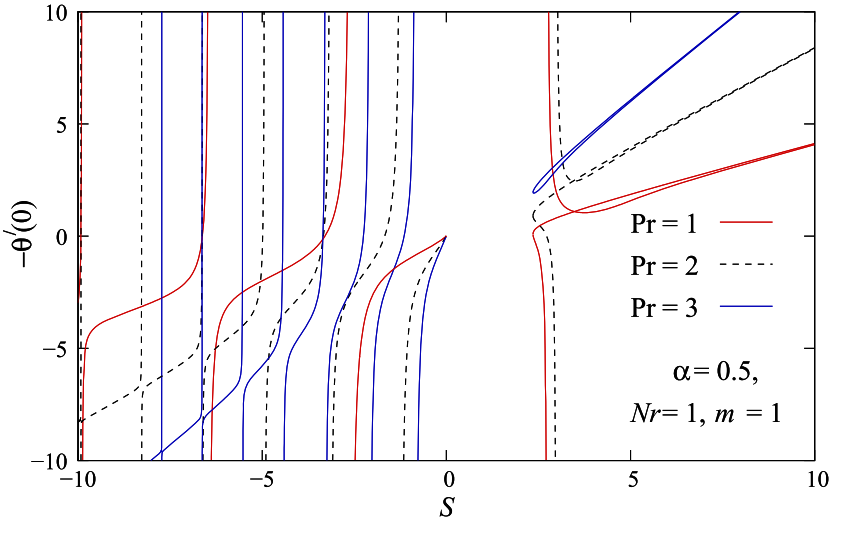

Figure 13. Nusselt number $Nu_x Re_x^{-1/2} = -\theta'(0)$ vs. S for various values of Prandtl number Pr (for the second-grade fluid, $\alpha > 0$).

Now if $m = -1$, then

$$Nu_x Re_x^{-1/2} = -\theta'(0) = \frac{\Pr}{(1+\frac{4}{3}Nr)}\left(S-\frac{1}{\lambda}\right) + \frac{\Pr}{(1+\frac{4}{3}Nr)\lambda} \times \frac{M\left(2+\frac{\Pr}{(1+\frac{4}{3}Nr)\lambda}\left(S-\frac{1}{\lambda}\right), 2+\frac{\Pr}{(1+\frac{4}{3}Nr)\lambda}\left(S-\frac{1}{\lambda}\right), \frac{\Pr}{(1+\frac{4}{3}Nr)\lambda^2}\right)}{M\left(1+\frac{\Pr}{(1+\frac{4}{3}Nr)\lambda}\left(S-\frac{1}{\lambda}\right), 1+\frac{\Pr}{(1+\frac{4}{3}Nr)\lambda}\left(S-\frac{1}{\lambda}\right), \frac{\Pr}{(1+\frac{4}{3}Nr)\lambda^2}\right)}.$$

It is also well known that $M(a+1, a+1, z) = M(a, a, z)$.

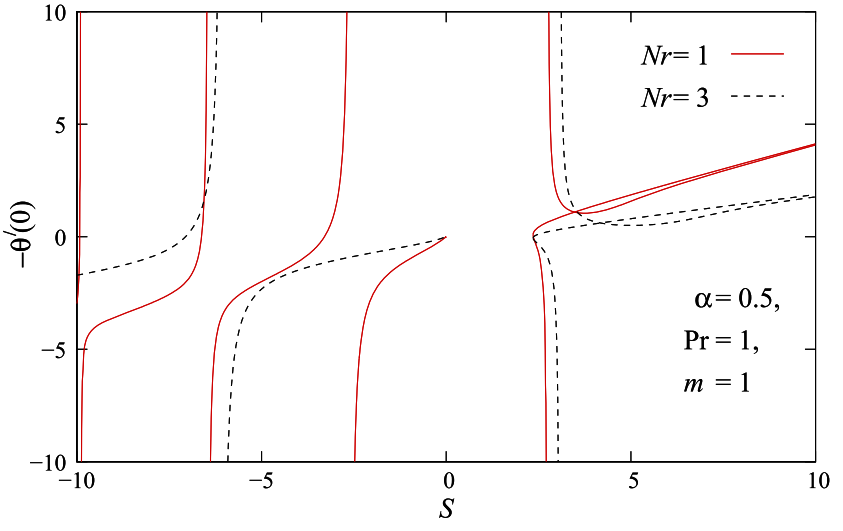

Figure 14. Nusselt number $Nu_x Re_x^{-1/2} = -\theta'(0)$ vs. S for various values of thermal radiation parameter Nr (for second-grade fluid, $\alpha > 0$).

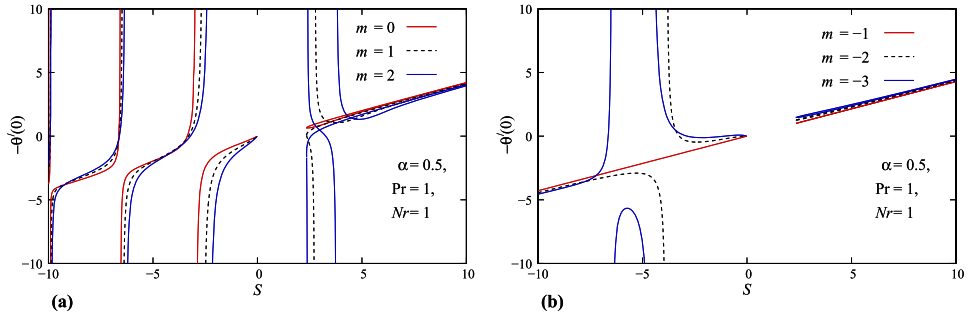

Figure 15. Nusselt number $Nu_x Re_x^{-1/2} = -\theta'(0)$ vs. S for various values of (a) $m \geq 0$ and (b) $m < 0$ (for the second-grade fluid, $\alpha > 0$).

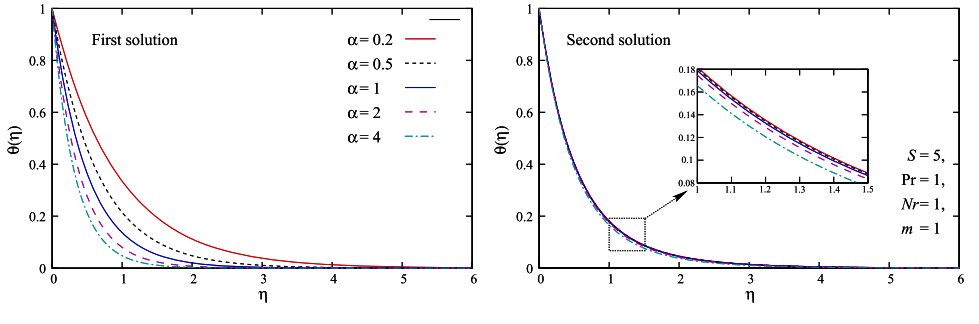

Figure 16. Temperature profiles for various values of viscoelastic parameter α (for the second-grade fluid, $\alpha > 0$).

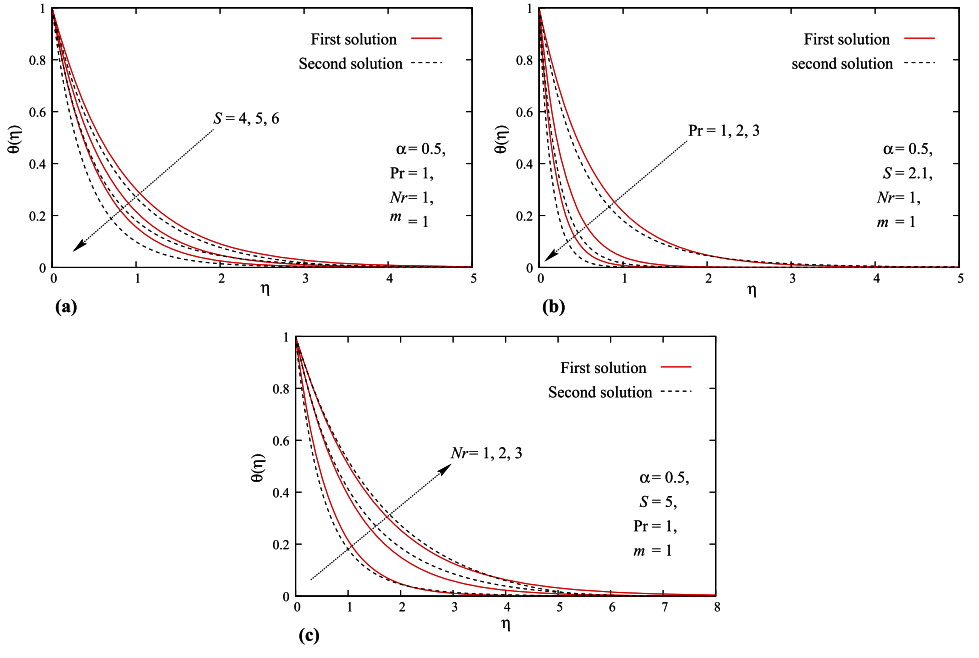

Figure 17. Temperature profiles for various values of (a) suction parameter S, (b) Prandtl number Pr and (c) thermal radiation parameter Nr (for the second-grade fluid, $\alpha > 0$).

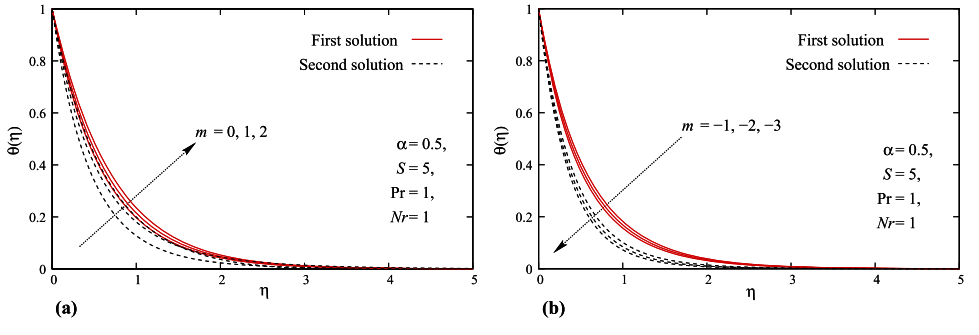

Figure 18. Temperature profiles for various values of (a) $m \geq 0$ and (b) $m < 0$ (for the second-grade fluid, $\alpha > 0$).

Hence, the expression of the local Nusselt number ultimately becomes

$$Nu_x \mathrm{Re}_x^{-1/2} = -\theta'(0) = \frac{\mathrm{Pr}}{(1+\frac{4}{3}Nr)}\left(S - \frac{1}{\lambda}\right) + \frac{\mathrm{Pr}}{(1+\frac{4}{3}Nr)\lambda} = \frac{S\,\mathrm{Pr}}{(1+\frac{4}{3}Nr)}.$$

It means that the local Nusselt number is independent of λ, i.e. if for some values of S and α, there exists multiple temperature profiles, the value of Nu_x is always the same for all solutions when $m = -1$. One more fact is coming out after this analysis that for $m = -1$ the Nusselt number, the rate of heat transfer is not even depending on α. So, the heat transfer can be fully controlled by the parameter m for any type of the viscoelastic fluid. Thus, if the surface temperature is inversely proportional along the sheet with linear power, then

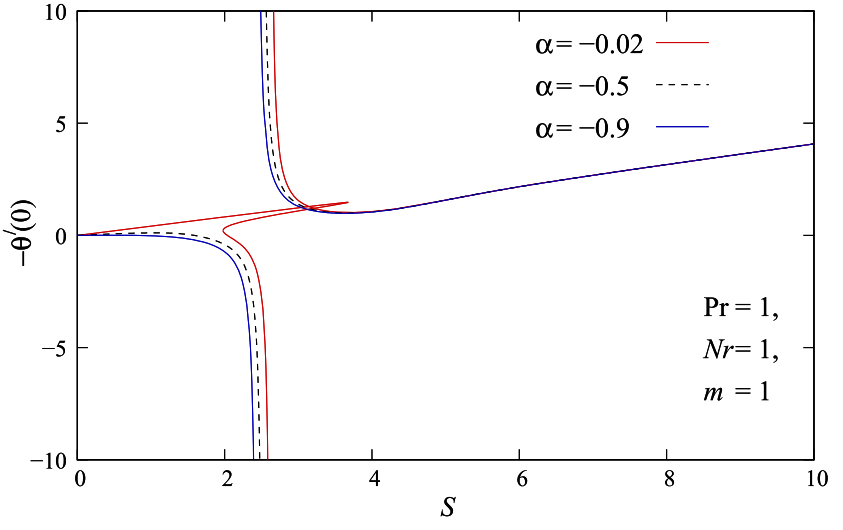

Figure 19. Nusselt number $Nu_x Re_x^{-1/2} = -\theta'(0)$ vs. S for various values of viscoelastic parameter α (for Walter's liquid B, $\alpha < 0$).

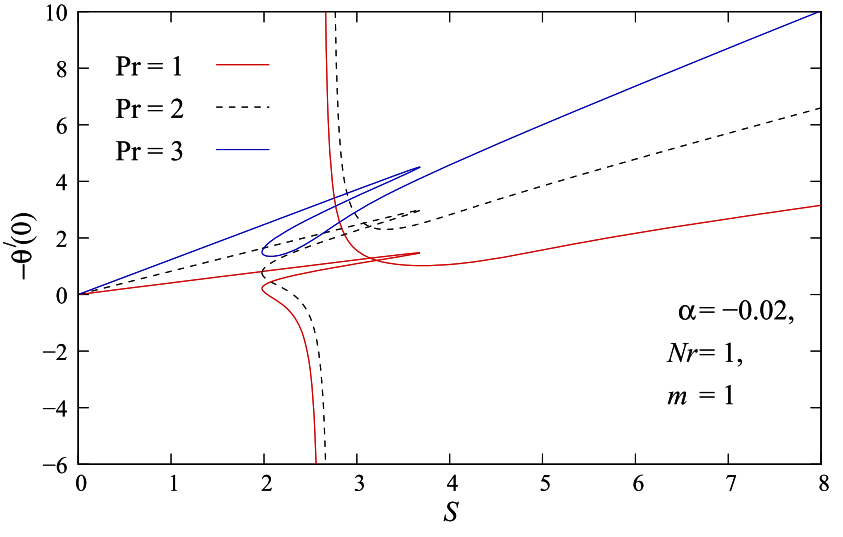

Figure 20. Nusselt number $Nu_x Re_x^{-1/2} = -\theta'(0)$ vs. S for various values of Prandtl number Pr (for Walter's liquid B, $\alpha < 0$).

heat transfer from the sheet will be constant for various types of viscoelastic fluids. The effects of various involved physical parameters on Nussult number and temperature profiles are explored in Figures 12–25 for second-grade fluid and Walter's liquid B. Dual and single solutions for second-grade fluid and triple and single solutions for Walter's liquid B in temperature distribution are reported. All the parameters that are representatives of some physical properties have significant impacts on the temperature field and the heat transfer rate similar to the velocity. It is important to note that though the Nusselt number,

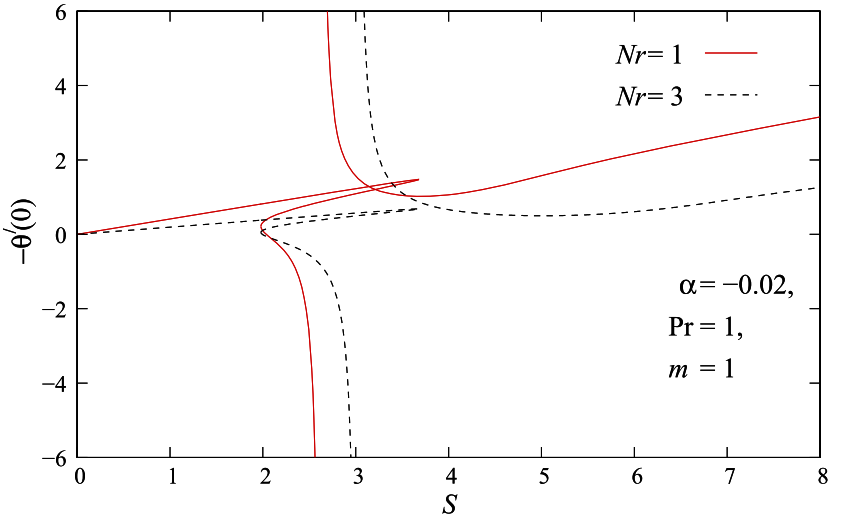

Figure 21. Nusselt number $Nu_x Re_x^{-1/2} = -\theta'(0)$ vs. S for various values of thermal radiation parameter Nr (for Walter's liquid B, $\alpha < 0$).

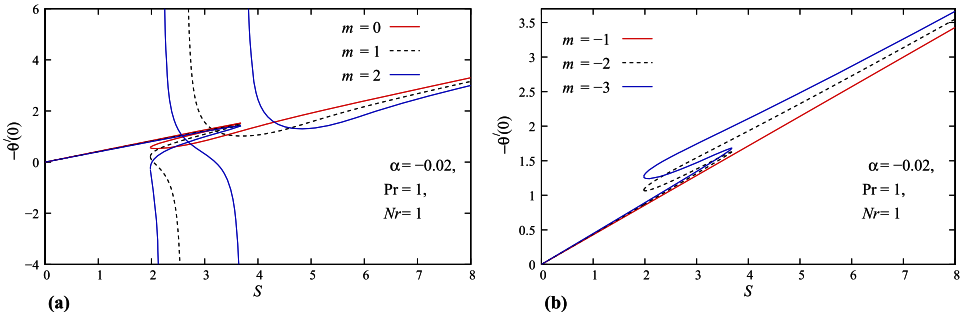

Figure 22. Nusselt number $Nu_x Re_x^{-1/2} = -\theta'(0)$ vs. S for various values of (a) $m \geq 0$ and (b) $m < 0$ (for Walter's liquid B, $\alpha < 0$).

i.e. the heat transfer rate, is constant for various viscoelastic fluids when $m = -1$, but the temperature profiles are not the same.

4. Conclusions

The flow of two classes of viscoelastic fluids and heat transfer due to the shrinking of a permeable sheet with thermal radiation and variable surface temperature is studied. Along with the unique solution, multiple exact similarity solutions are obtained. After a detail analytical investigation, the following key points can be summarized as follows:

(a) Along with single solution, the dual closed-form solutions of the flow field and temperature are reported in some specific flow situations of the second-grade fluid.

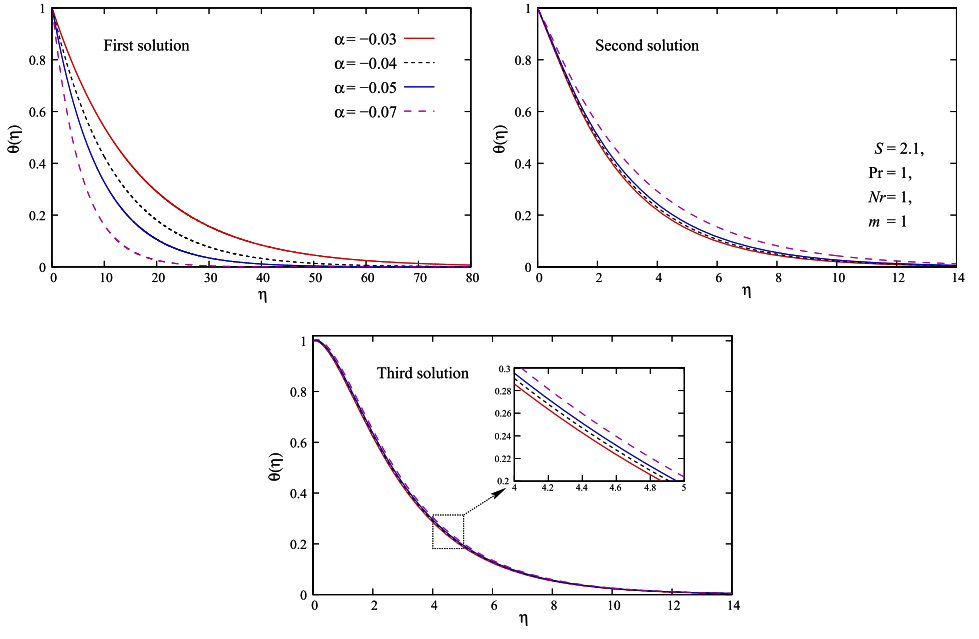

Figure 23. Triple temperature profiles for various values of viscoelastic parameter α (for Walter's liquid B, $\alpha < 0$).

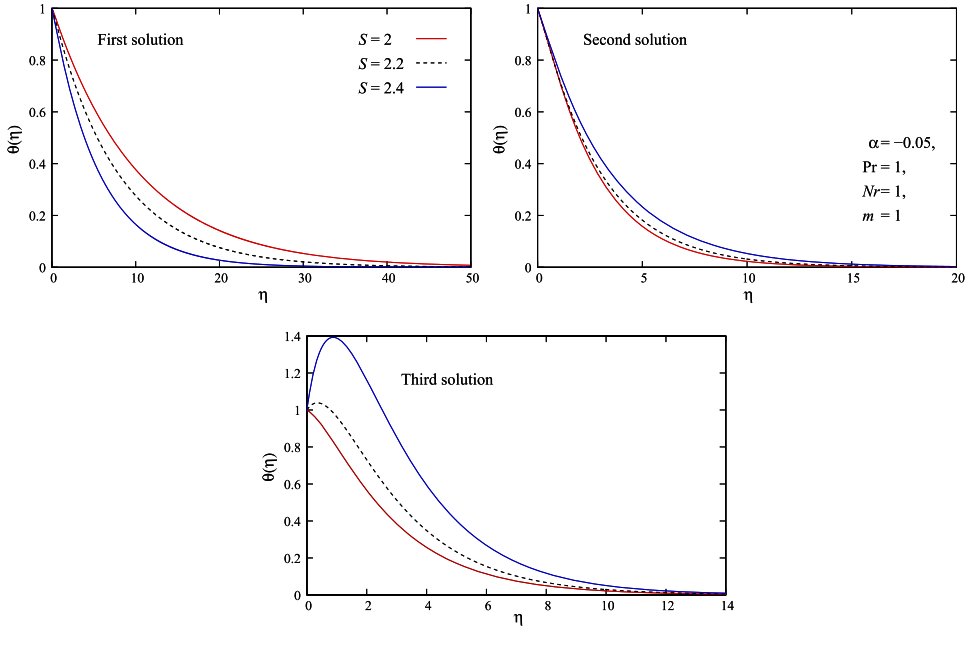

Figure 24. Triple temperature profiles for various values of suction parameter S (for Walter's liquid B, $\alpha < 0$).

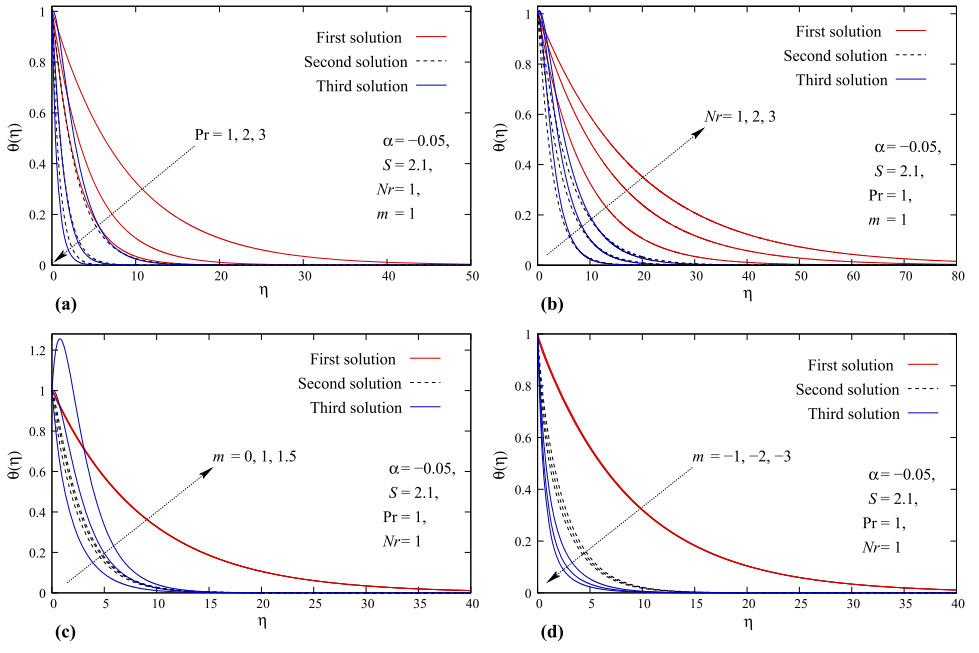

Figure 25. Triple temperature profiles for various values of (a) Pr, (b) *Nr*, (c) $m \geq 0$ and (d) $m < 0$ (for Walter's liquid B, $\alpha < 0$).

(b) For Walters liquid B, the triple closed-form solutions are obtained in addition to unique solution for specific values of flow parameters.

(c) Unique self-similar solution for the second-grade fluid flow is noticed when there is a mass injection and some interval of no solution for weaker mass suction along with dual solutions for stronger cases are found. While, for the flow of Walters liquid B, self-similar solution is attained only for mass suction (weak or strong).

(d) Dual exact solutions for energy equation are also obtained in terms of Kummer function for both types of fluids.

(e) The heat transfer rate is independent of viscoelastic parameter α (i.e. fluid rheology) if surface temperature distribution is supposed to inversely proportional along the sheet.

Acknowledgements

The authors are thankful to the anonymous reviewers for their constructive suggestions and comments.

Disclosure statement

No potential conflict of interest was reported by the author(s).

Funding

The research of A.K. Verma is funded by Council of Scientific and Industrial Research [grant number 09/013 (0724)/2017-EMR-I] and the work of A.K. Gautam is supported by University Grants Commission [grant number 1220/(CSIR-UGC NET DEC. 2016)].

ORCID

Krishnendu Bhattacharyya http://orcid.org/0000-0001-7975-0709

References

[1] Siddappa AB, Khapate BS. Rivlin-Ericksen fluid flow past a stretching plate. Rev Roum Sci Tech Mech Appl. 1976;21:497–505.
[2] Rajagopal KR, Na TY, Gupta AS. Flow of a viscoelastic fluid over a stretching sheet. Rheol Acta. 1984;23:213–215.
[3] Siddappa AB, Abel MS. Non-Newtonian flow past a stretching plate. Z Angew Math Phys. 1985;36:890–892.
[4] Siddappa B, Abel MS. Visco-elastic boundary layer flow past a stretching plate with suction and heat transfer. Rheol Acta. 1986;25:319–320.
[5] Dandapat BS, Gupta AS. Flow and heat transfer in a viscoelastic fluid over a stretching sheet. Int J Non-Linear Mech. 1989;24:215–219.
[6] Ahmad AN, Patel GS, Siddappa B. Visco-elastic boundary layer flow past a stretching plate and heat transfer. Z Angew Math Phys. 1990;41:294–298.
[7] Andersson HI. MHD flow of a viscoelastic fluid past a stretching surface. Acta Mech. 1992;95:227–230.
[8] Cortell AR. Similarity solutions for flow and heat transfer of a viscoelastic fluid over a stretching sheet. Int J Non-Linear Mech. 1994;29:155–161.
[9] Vajravelu BK, Roper T. Flow and heat transfer in a second grade fluid over a stretching sheet. Int J Non-Linear Mech. 1999;34:1031–1036.
[10] Cortell CR. A note on flow and heat transfer of a viscoelastic fluid over a stretching sheet. Int J Non-Linear Mech. 2006;41:78–85.
[11] Sarma MS, Rao BN. Heat transfer in a viscoelastic fluid over a stretching sheet. J Math Anal Appl. 1998;222:268–275.
[12] Ariel PD. Axisymmetric flow of a second grade fluid past a stretching sheet. Int J Eng Sci. 2001;39:529–553.
[13] Khan SK, Abel MS, Sonth RM. Viscoelastic MHD flow, heat and mass transfer over a porous stretching sheet with dissipation of energy and stress work. Heat Mass Transf. 2003;40:47–57.
[14] Hayat AT, Sajid M. Analytic solution for axisymmetric flow and heat transfer of a second grade fluid past a stretching sheet. Int J Heat Mass Transf. 2007;50:75–84.
[15] Cortell BR. MHD flow and mass transfer of an electrically conducting fluid of second grade in a porous medium over a stretching sheet with chemically reactive species. Chem Eng Process. 2007;46:721–728.
[16] Bataller RC. Viscoelastic fluid flow and heat transfer over a stretching sheet under the effects of a non-uniform heat source, viscous dissipation and thermal radiation. Int J Heat Mass Transf. 2007;50:3152–3162.
[17] Abel MS, Nandeppanavar MM, Malipatil SB. Heat transfer in a second grade fluid through a porous medium from a permeable stretching sheet with non-uniform heat source/sink. Int J Heat Mass Transf. 2010;53:1788–1795.
[18] Chen C-H. On the analytic solution of MHD flow and heat transfer for two types of viscoelastic fluid over a stretching sheet with energy dissipation, internal heat source and thermal radiation. Int J Heat Mass Transf. 2010;53:4264–4273.
[19] Cortell AR. Toward an understanding of the motion and mass transfer with chemically reactive species for two classes of viscoelastic fluid over a porous stretching sheet. Chem Eng Process. 2007;46:982–989.
[20] Turkyilmazoglu BM. The analytical solution of mixed convection heat transfer and fluid flow of a MHD viscoelastic fluid over a permeable stretching surface. Int J Mech Sci. 2013;77:263–268.
[21] Hayat CT, Hussain Z, Farooq M, et al. Effects of homogeneous and heterogeneous reactions and melting heat in the viscoelastic fluid flow. J Mol Liq. 2016;215:749–755.

[22] Hayat DT, Abbas Z, Sajid M. On the analytic solution of magnetohydrodynamic flow of a second grade fluid over a shrinking sheet. ASME J Appl Mech. 2007;74:1165–1171.
[23] Naganthran EK, Nazar R, Pop I. Stability analysis of impinging oblique stagnation-point flow over a permeable shrinking surface in a viscoelastic fluid. Int J Mech Sci. 2017;131-132:663–671.
[24] Miklavčič FM, Wang CY. Viscous flow due a shrinking sheet. Q Appl Math. 2006;64:283–290.
[25] Seth GS, Singha AK, Mandal MS, et al. MHD stagnation-point flow and heat transfer past a non-isothermal shrinking/stretching sheet in porous medium with heat sink or source effect. Int J Mech Sci. 2017;134:98–111.
[26] Bhatti MM, Ali Abbasb M, Rashidi MM. A robust numerical method for solving stagnation point flow over a permeable shrinking sheet under the influence of MHD. Appl Math Comput. 2018;316:381–389.
[27] Ahmad AS, Yousaf M, Khan A, et al. Magnetohydrodynamic fluid flow and heat transfer over a shrinking sheet under the influence of thermal slip. Heliyon. 2018;4:e00828.
[28] Merkin JH, Pop I. Stagnation point flow past a stretching/shrinking sheet driven by Arrhenius kinetics. Appl Math Comput. 2018;337:5830–5590.
[29] Ismail NS, Arifin NM, Nazar R, et al. Stability analysis of unsteady MHD stagnation point flow and heat transfer over a shrinking sheet in the presence of viscous dissipation. Chin J Phys. 2019;57:116–126.
[30] Mahabaleshwar US, Nagaraju KR, Sheremet MA, et al. Mass transpiration on Newtonian flow over a porous stretching/shrinking sheet with slip. Chin J Phys. 2020;63:130–137.
[31] Ali A, Marwat DNK. Force convective flow over a porous and stretching (shrinking) sheet of variable thickness. J Therm Anal Calorim. 2021;143:3559–3567.
[32] Lemini DG. Engineering viscoelasticity. New York: Springer; 2014.
[33] Yu J, Sakai S, Sethian JA. Two-phase viscoelastic jetting. J Comput Phys. 2007;220:568–585.
[34] Garg VK, Rajagopal KR. Flow of non-Newtonian fluid past a wedge. Acta Mech. 1992;93:53–61.
[35] Seddeek MA, Abdelmeguid MS. Effects of radiation and thermal diffusivity on heat transfer over a stretching surface with variable heat flux. Phys Lett A. 2006;348:172–179.
[36] Mukhopadhyay S, Layek GC. Effects of thermal radiation and variable fluid viscosity on free convective flow and heat transfer past a porous stretching surface. Int J Heat Mass Transf. 2008;51:2167–2178.
[37] Abramowitz M, Stegun F. Handbook of mathematical functions with formulas, graphs and mathematical tables. Washington, DC: Dover Publications; 1972.